Supporting Information for

Mn^{IV}-oxo Complex of a Bis(benzimidazolyl)-containing N5 Ligand Reveals Different Reactivity Trends for Mn^{IV}-oxo than Fe^{IV}-oxo Species

Melissa C. Denler,[a,±] Allyssa A. Massie,[a,±] Reena Singh,[b] Eleanor Stewart-Jones,[a] Arup Sinha,[b] Victor W. Day, [a] Ebbe Nordlander,[b] and Timothy A. Jackson[*a]

[a] *The University of Kansas, Department of Chemistry and Center for Environmentally Beneficial Catalysis, 1567 Irving Hill Road , Lawrence, KS 66045, USA.* [b] *Lund University, Chemical Physics, Department of Chemistry, Box 124, SE-221 00 Lund, Sweden.*

± These authors made contributions of equal merit.

Content

S.1 ***XRD Data for $Mn^{II}(OH_2)(2pyN2B)](OTf)_2$.*** A checkCIF A-alert for $Mn^{II}(OH_2)(2pyN2B)](OTf)_2$ is likely due to a slight disordering of the ether solvent molecule of crystallization. This disorder produces larger thermal parameters for its atoms than those of the metal complex. The structure of $[Mn^{II}(OH_2)(2pyN2B)](ClO_4)_2 \bullet 2CH_3CN$ was also determined (CCDC entry 1891620).

S.2 ***Synthesis and Characterization of $[Mn^{II}(OH_2)(2pyN2B)](ClO_4)_2$.*** To a MeCN solution (10 ml) of the ligand (0.047 g, 0.1 mmol), $Mn(ClO_4)_2.6H_2O$ was added and the solution turned pale green. This solution was stirred for 4 hours and was left for slow evaporation of MeCN. After 4-5 days, white colored crystals were isolated. The crystals were washed with MeCN to remove any excess ligand. Crystals were obtained by slow evaporation in MeCN. ESI-MS data for $[Mn(OH_2)(2pyN2B)](ClO_4)_2$ dissolved in MeCN show the following peaks (m/z): 264.02 corresponding to $[Mn^{II}(2pyN2B)]^{2+}$ (calculated 264.08), 563.05 corresponding to $[Mn(2pyN2B)(OH)(H_2O)]^{+}$ (calculated 563.18) and 627.02 corresponding to $[Mn(2pyN2B)(OH)(H_2O)(CH3OH)_2]^{+}$ (calculated 627.23).The bond parameters of this structure do not differ significantly from $[Mn^{II}(OH_2)(2pyN2B)](OTf)_2$ (see Table S2).

Table S1. Crystal Data and Structure Refinement

Identification	$Mn^{II}(OH_2)(2pyN2B)](OTf)_2$	
CCDC Identification Code	1874429	
Empirical formula	$C_{35}H_{39}F_6MnN_7O_8S_2$	
Formula weight	918.79	
Temperature	228 K	
Wavelength	0.71073 Å	
Crystal system	Orthorhombic	
Space group	Pnma – D_{2h}^{16} (No. 62)	
Unit cell dimensions	**a** = 19.166(2) Å	**α** = 90.000°
	b = 19.200(2) Å	**β** = 90.000°
	c = 11.2881(12) Å	**γ** = 90.000°
Volume	4153.9(8) $Å^3$	
Z	4	
Density (calculated)	1.469 g/cm^3	
Absorption coefficient	0.50 mm^{-1}	
F(000)	1892	
Crystal size	0.450 x 0.180 x 0.180 mm^3	
Theta range for data collection	2.125 to 28.280°.	
Index ranges	$-25 \leq h \leq 25$, $-25 \leq k \leq 25$, $-15 \leq l \leq 15$	
Reflections collected	55690	
Independent reflections	5299 [R_{int} = 0.059]	
Completeness to theta = 27.500°	99.9 %	
Absorption correction	Multi-scan	
Max. and min. transmission	1.000 and 0.768	
Refinement method	Full-matrix least-squares on F^2	
Data / restraints / parameters	5299 / 0 / 331	
Goodness-of-fit on F^2	1.053	
Final R indices [I>2sigma(I)]	R_1 = 0.048, wR_2 = 0.124	
R indices (all data)	R_1 = 0.071, wR_2 = 0.145	
Extinction coefficient	n/a	
Largest diff. peak and hole	0.53 and -0.45 $e^-/Å^3$	

Table S2. Comparison of Structural Properties of perchlorate and triflate salts of $[Mn^{II}(OH_2)(2pyN2B)]^{2+}$.

	$[Mn^{II}(OH_2)(2pyN2B)](ClO_4)_2$	$[Mn^{II}(OH_2)(2pyN2B)](OTf)_2$
CCDC Entry Number	1891620	1874429
Mn–O	2.076(7)	2.087(3)
$Mn–N_{benzimidazolyl}$	2.181(5)	2.193(2)
$Mn–N_{benzimidazolyl}$	2.181(5)	2.193(2)
$Mn–N_{pyridyl}$	2.311(5)	2.298(2)
$Mn–N_{pyridyl}$	2.311(5)	2.298(2)
$Mn–N_{amine}$	2.353(7)	2.375(3)
$Mn–N_{equatorial}$ [b]	2.246	2.246
$Mn–N_{total}$ [c]	2.267	2.271

[a] Average of the Mn–N bond distances in the equatorial positions. [b] Average of all Mn–N bond distances.

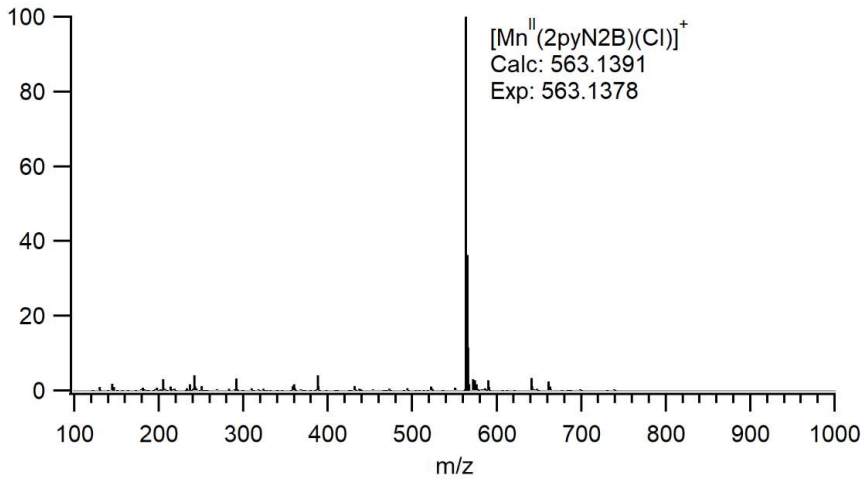

Figure S1. ESI-MS of $[Mn^{II}(OH_2)(2pyN2B)](OTf)_2$.

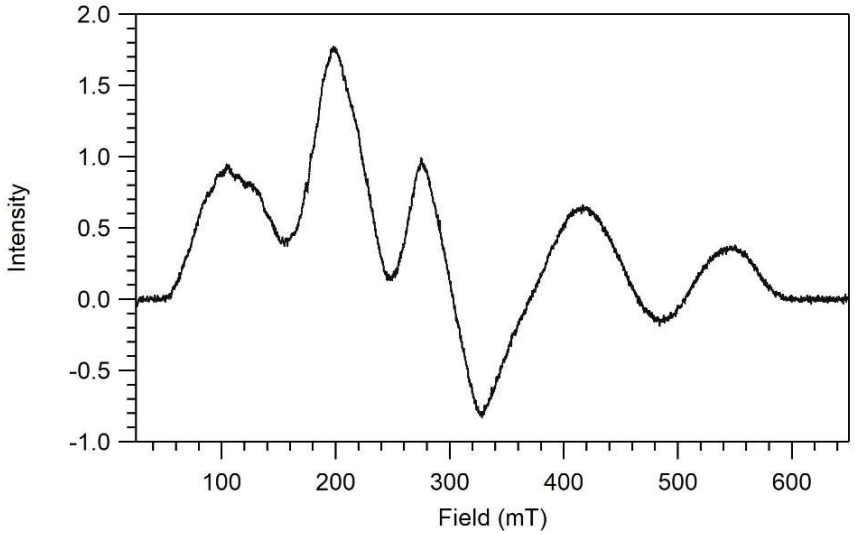

Figure S2. Perpendicular mode EPR of 1 mM $[Mn^{II}(OH_2)(2pyN2B)](OTf)_2$ in TFE at 10K.

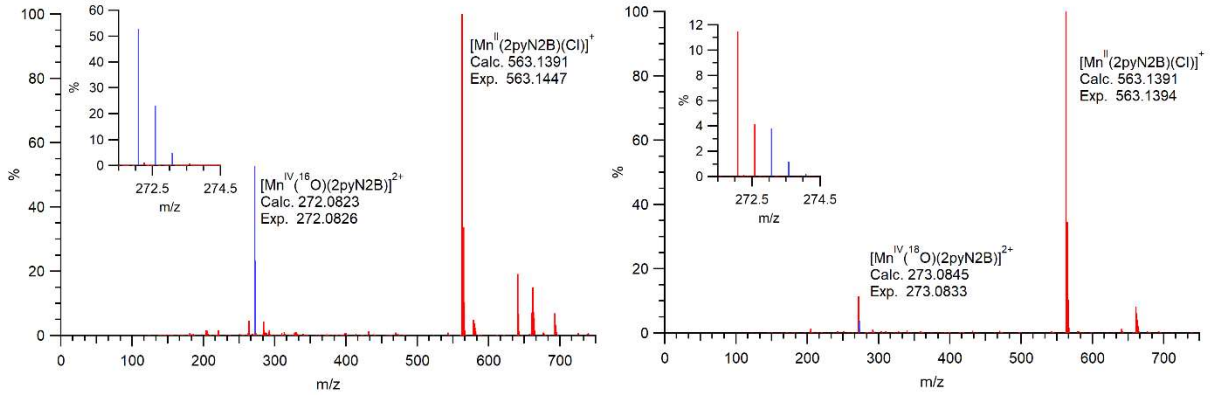

Figure S3. ESI-MS of $[Mn^{IV}(^{16}O)(2pyN2B)]^{2+}$ (left) and $[Mn^{IV}(^{18}O)(2pyN2B)]^{2+}$ (right).

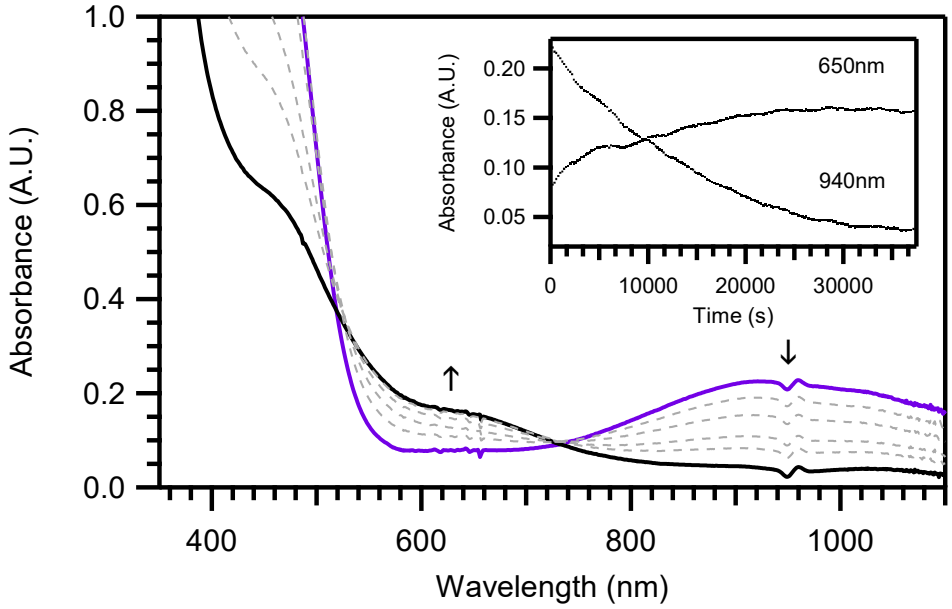

Figure S4. Electronic absorption spectra showing the thermal decay of 1 mM $[Mn^{IV}(O)(2pyN2B)]^{2+}$ in TFE at 25 °C.

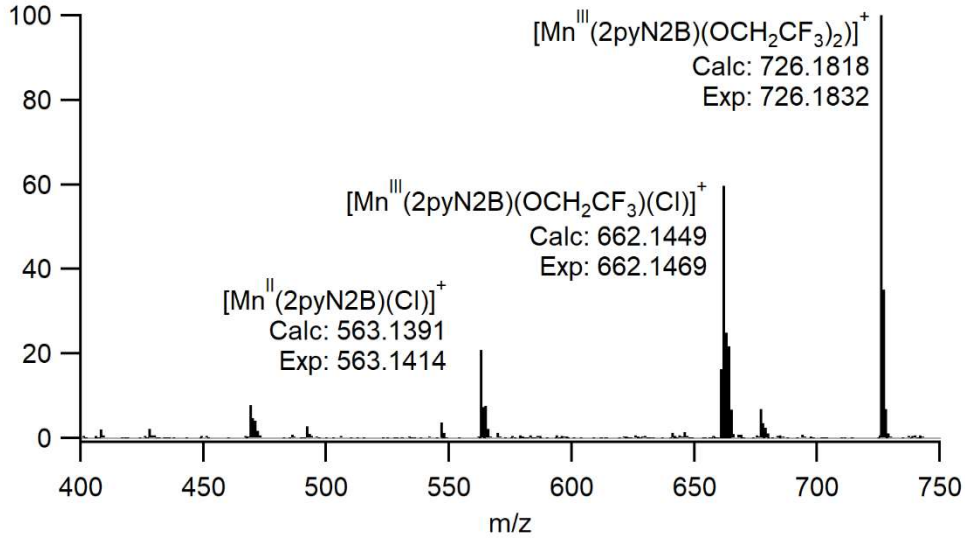

Figure S5. ESI-MS of the self decay of 1 mM $[Mn^{IV}(O)(2pyN2B)]^{2+}$ in TFE.

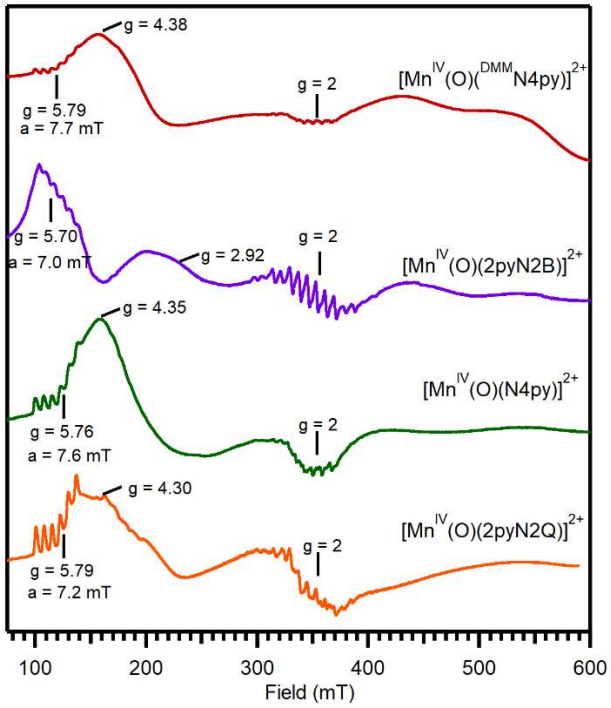

Figure S6. Perpendicular-mode X-band EPR spectra of $[Mn^{IV}(O)(^{DMM}N4py)]^{2+}$, $[Mn^{IV}(O)(2pyN2B)]^{2+}$, $[Mn^{IV}(O)(N4py)]^{2+}$, and $[Mn^{IV}(O)(2pyN2Q)]^{2+}$. All experiments were carried out at 5 K, except that of $[Mn^{IV}(O)(2pyN2B)]^{2+}$, which was collected at 10 K. Data for $[Mn^{IV}(O)(^{DMM}N4py)]^{2+}$, $[Mn^{IV}(O)(N4py)]^{2+}$, and $[Mn^{IV}(O)(2pyN2Q)]^{2+}$ are from references [1] and [2].

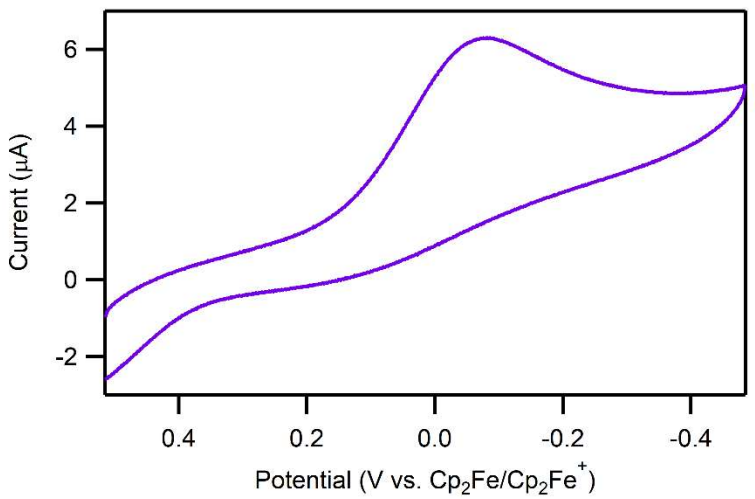

Figure S7. Cyclic voltammogram of $[Mn^{IV}(O)(2pyN2B)]^{2+}$ recorded in TFE with 0.1 M Bu_4NPF_6 electrolyte solution at 50 mV s^{-1}.

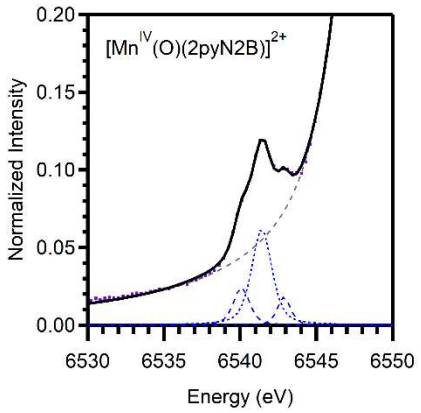

Figure S8. Comparison of the normalized XAS pre-edge data (dotted line) and fits (solid line) for the $[Mn^{IV}(O)(2pyN2B)]^{2+}$. The dashed traces represent the fit of the background and fits to the pre-edge peak.

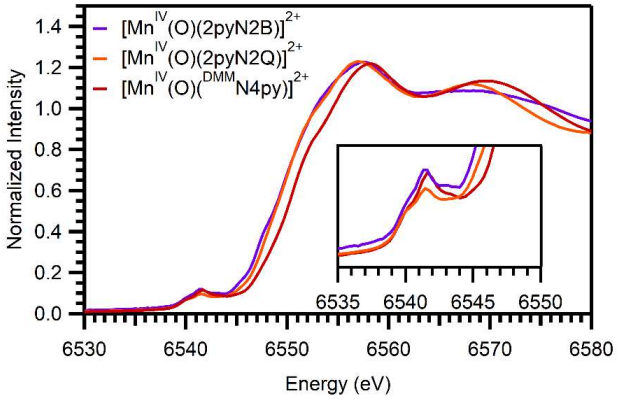

Figure S9. Comparison of experimental XANES regions for $[Mn^{IV}(O)(^{DMM}N4py)]^{2+}$, $[Mn^{IV}(O)(2pyN2B)]^{2+}$, and $[Mn^{IV}(O)(2pyN2Q)]^{2+}$.

Table S3. Selected Bond Lengths (Å) and Bond Angles for Oxomanganese(IV) Complexes $[Mn^{IV}(O)(N4py)]^{2+}$, $[Mn^{IV}(O)(^{DMM}N4py)]^{2+}$, $[Mn^{IV}(O)(2pyN2Q)]^{2+}$ and $[Mn^{IV}(O)(2pyN2Q)]^{2+}$ from DFT Computations.

	$[Mn^{IV}(O)(2pyN2B)]^{2+}$	$[Mn^{IV}(O)(N4py)]^{2+}$	$[Mn^{IV}(O)(^{DMM}N4py)]^{2+a}$	$[Mn^{IV}(O)(2pyN2Q)]^{2+a}$
Mn–O	1.671	1.673	1.678	1.678
Mn–N_X [b]	1.974	2.025	1.988	2.066
Mn–N_X [b]	1.974	2.026	1.989	2.066
Mn–$N_{pyridyl}$	2.047	2.012	2.041	2.043
Mn–$N_{pyridyl}$	2.048	2.011	2.041	2.042
Mn–N_{amine}	2.174	2.118	2.108	2.109
Mn–$N_{equatorial}$ [c]	2.011	2.018	2.015	2.054
Mn–N_{total} [d]	2.043	2.038	2.033	2.065
N_{amine}–Mn=O	177.48	179.55	179.76	170.63

[a] From reference 1. [b] N_X is $N_{benzimidazolyl}$ for $[Mn^{II}(OH_2)(2pyN2B)]^{2+}$, $N_{pyridyl}$ for $[Mn^{II}(OTf)(N4py)]^{+}$, $N_{3,5\text{-dimethyl-4-methoxypyridyl}}$ for $[Mn^{II}(OTf)(^{DMM}N4py)]^{+}$, and $N_{quinolinyl}$ for $[Mn^{II}(OH_2)(2pyN2Q)]^{2+}$. [c] Average of the Mn–N bond distances in the equatorial positions. [d] Average of all Mn–N bond distances.

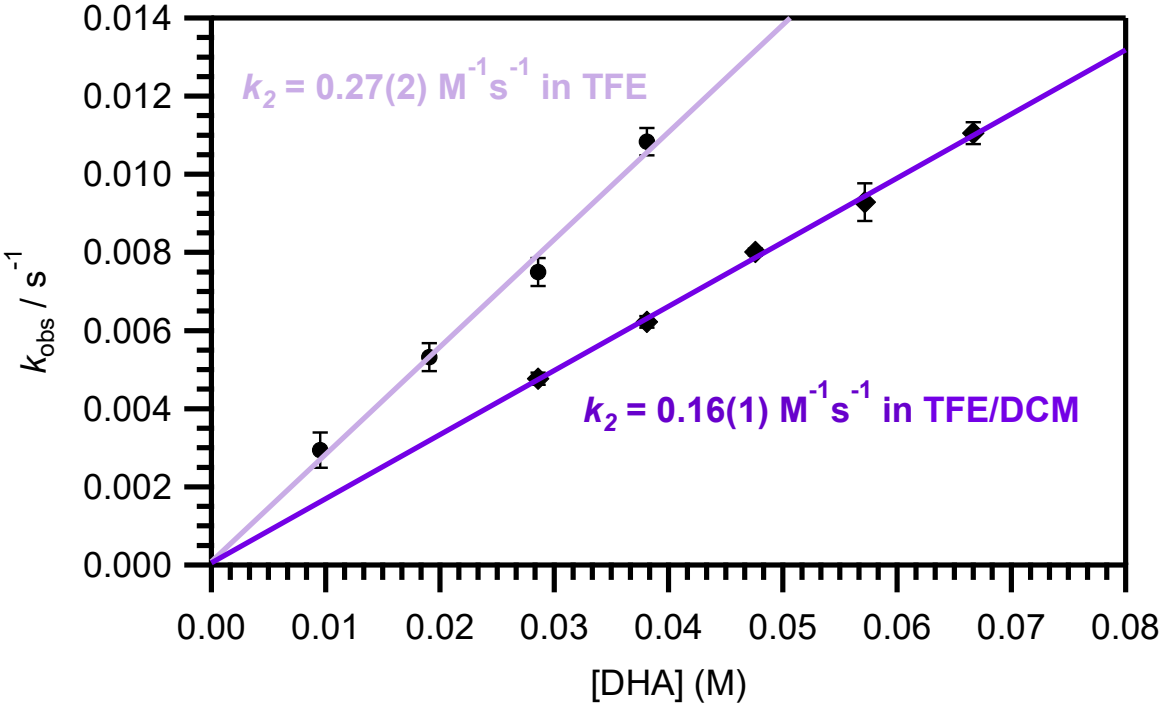

Figure S10. Pseudo-first-order rate constants (k_{obs}) vs. DHA concentration for $[Mn^{IV}(O)(2pyN2B)]^{2+}$ in TFE and TFE/DCM at 25 °C. The lines represent best fits to the data used to determine the second-order rate constants (k_2).

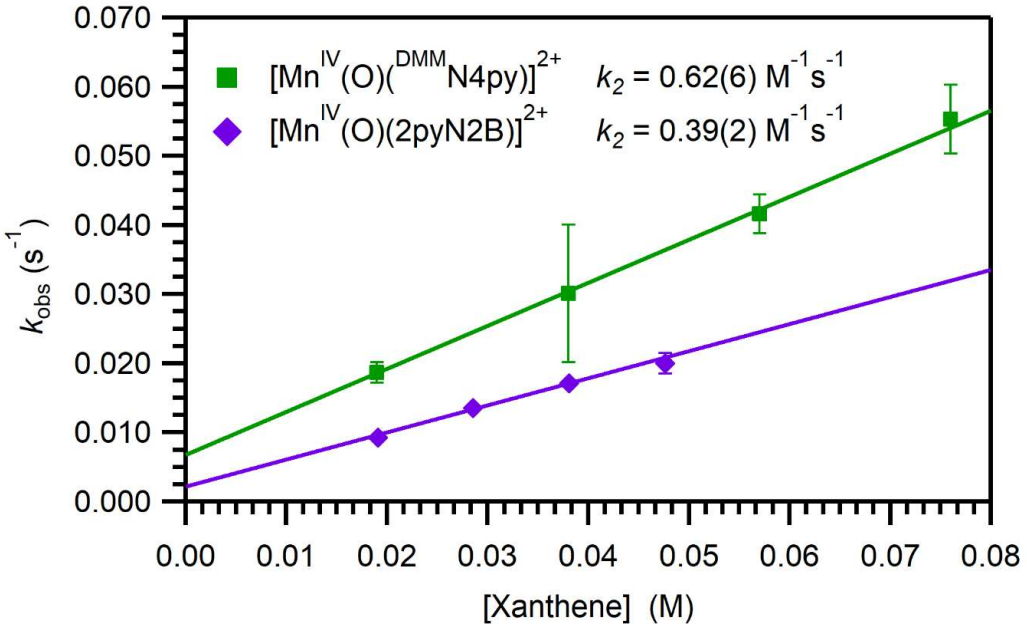

Figure S11. Pseudo-first order rate constants (k_{obs}) vs. xanthene concentration for $[Mn^{IV}(O)(2pyN2B)]^{2+}$ (purple) and for $[Mn^{IV}(O)(^{DMM}N4py)]^{2+}$ (green) in 1:1 TFE:CH_2Cl_2 at 25 °C. The lines represent best fits to the data used to determine the second-order rate constants (k_2).

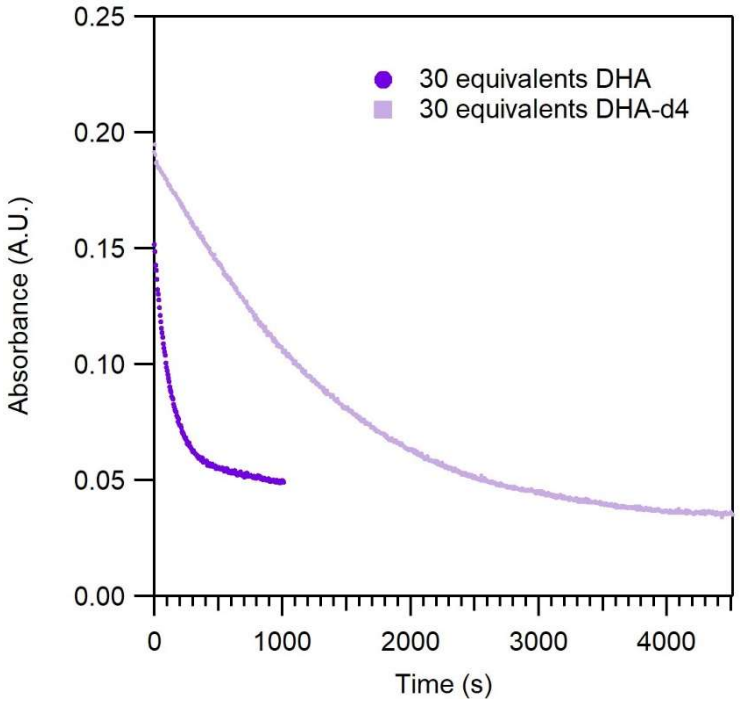

Figure S12. Time trace of the decay of the 940 nm electronic absorption signal of a 1 mM solution of $[Mn^{IV}(O)(2pyN2B)]^{2+}$ in TFE at 25 °C upon the addition of 30 equivalents DHA dark purple circles) and [D_4]-DHA (light purple squares).

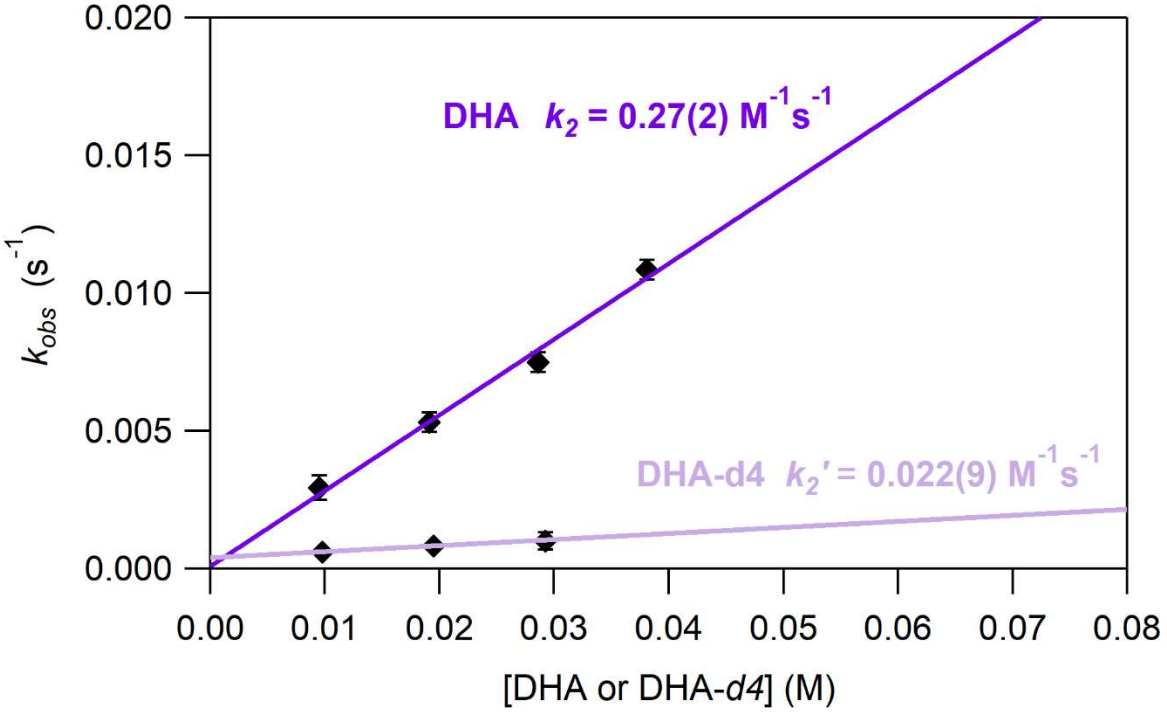

Figure S13. Pseudo-first order rate constants (k_{obs}) vs. DHA (dark purple) and DHA-d4 (light purple) $[Mn^{IV}(O)(2pyN2B)]^{2+}$ in TFE at 25 °C. The lines represent best fits to the data used to determine the second-order rate constants (k_2).

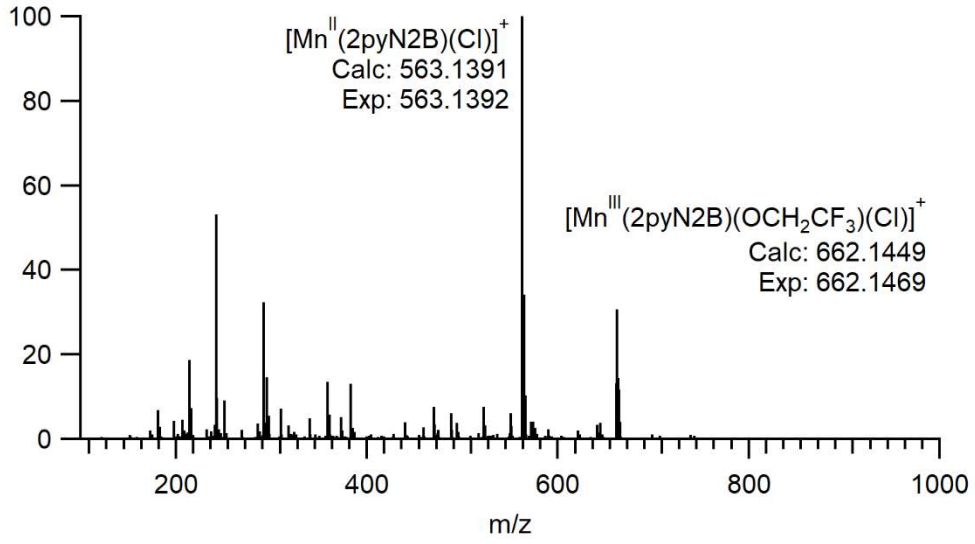

Figure S14. ESI-MS following the reaction of 1.0 mM $[Mn^{IV}(O)(2pyN2B)]^{2+}$ in TFE with 40 equivalents of DHA.

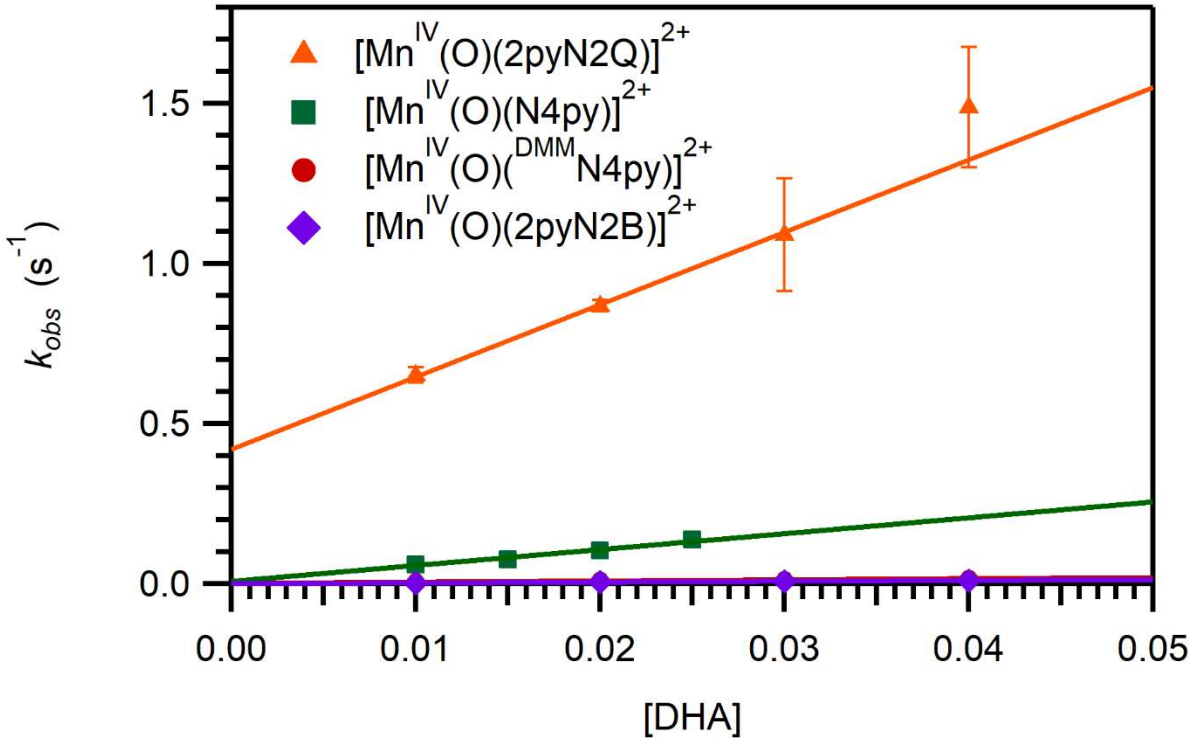

Figure S15. Pseudo-first-order rate constants (k_{obs}) versus DHA concentration for oxomanganese(IV) species, showing experimental data for $[Mn^{IV}(O)(2pyN2Q)]^{2+}$. Rate data for $[Mn^{IV}(O)(^{DMM}N4py)]^{2+}$ and $[Mn^{IV}(O)(2pyN2Q)]^{2+}$ are from reference [1]; data for $[Mn^{IV}(O)(N4py)]^{2+}$ are from reference [2].

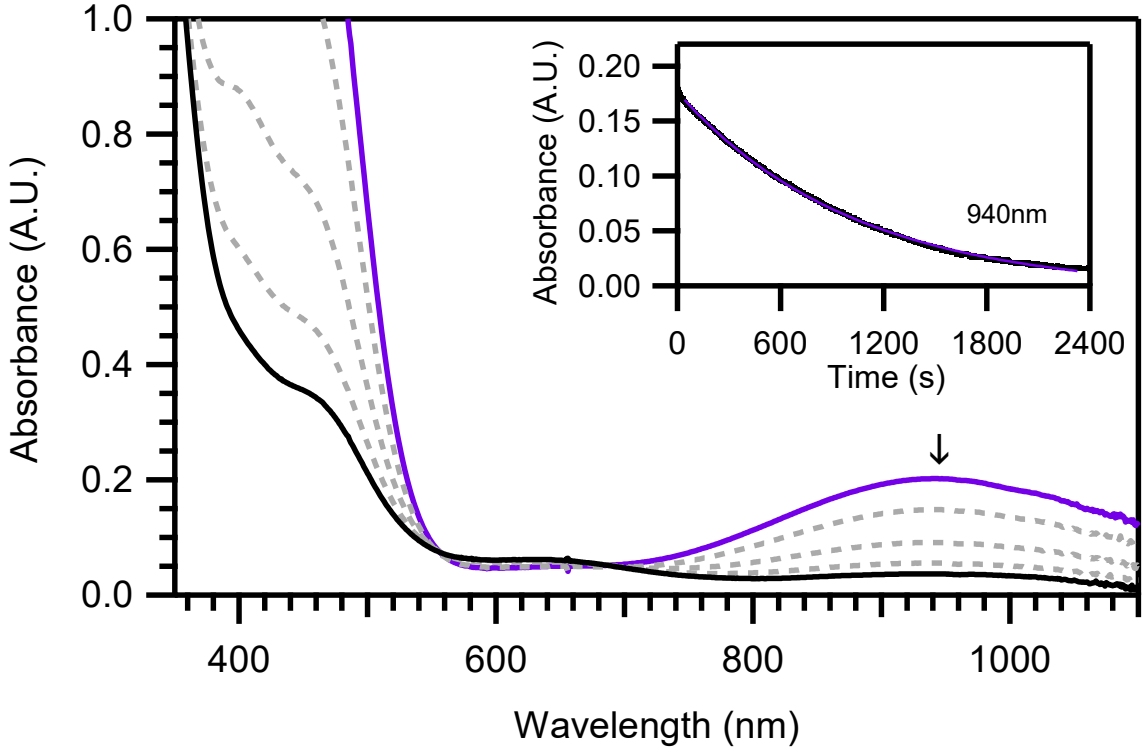

Figure S16. Electronic absorption spectra showing the reaction of 1.0 mM $[Mn^{IV}(O)(2pyN2B)]^{2+}$ (purple trace) with 40 equivalents of thioanisole in TFE at 25 °C. Inset: decay of the feature at 940nm over time.

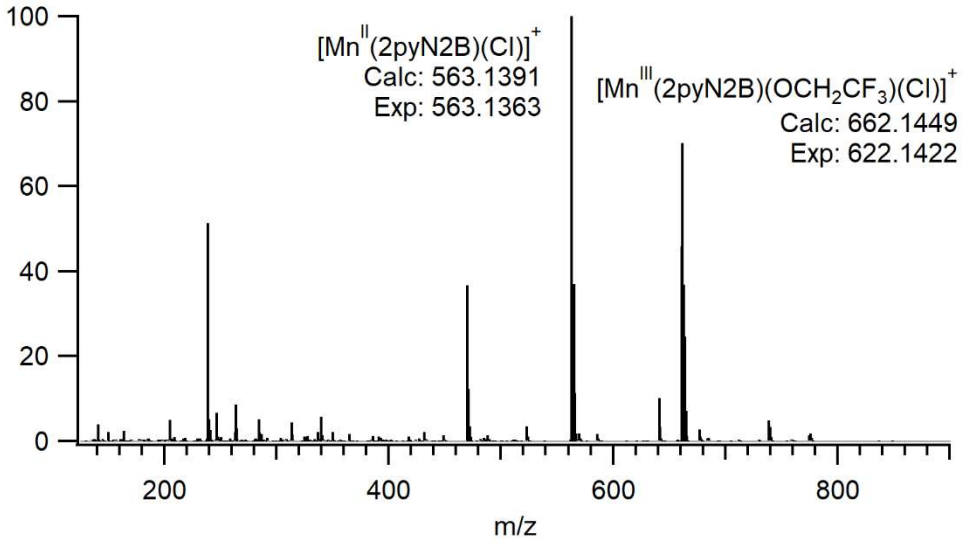

Figure S17. ESI-MS following the reaction of 1.0 mM $[Mn^{IV}(O)(2pyN2B)]^{2+}$ in TFE with 40 equivalents of thioanisole.

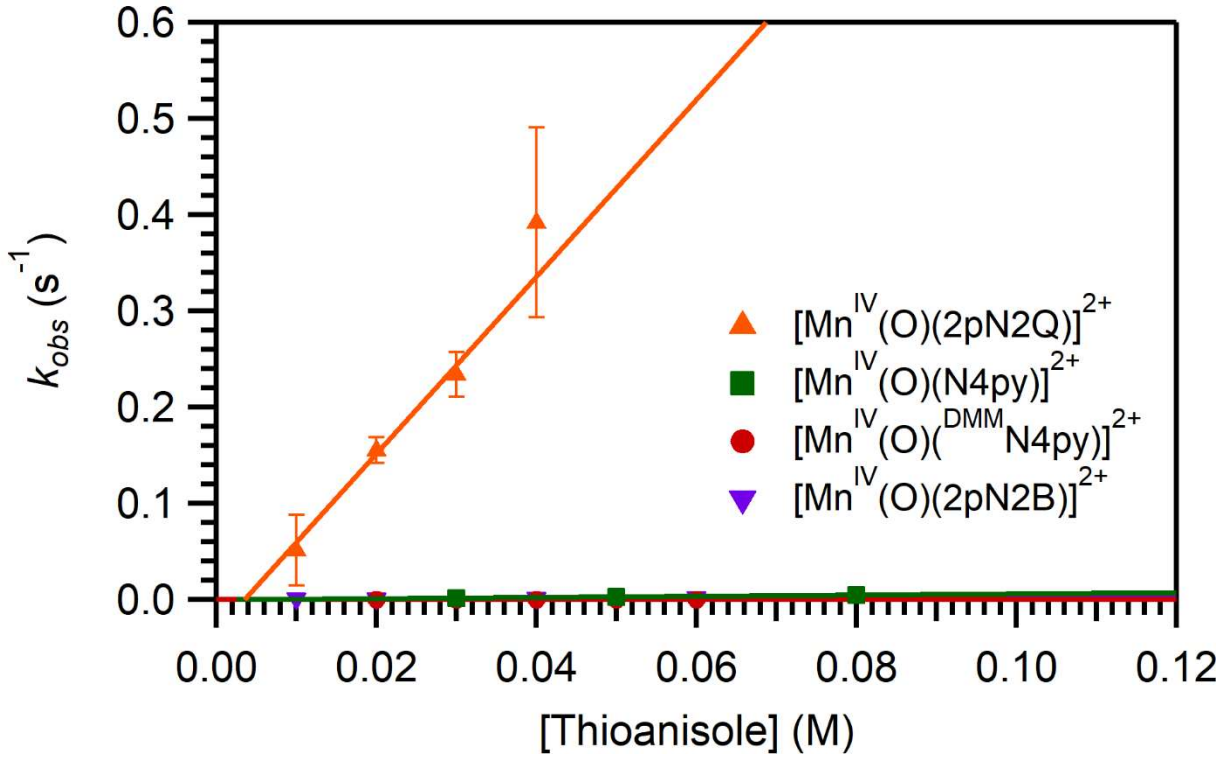

Figure S18. Pseudo-first-order rate constants (k_{obs}) versus thioanisole concentration for oxomanganese(IV) species showing experimental data for $[Mn^{IV}(O)(2pyN2Q)]^{2+}$. Rate data for $[Mn^{IV}(O)(^{DMM}N4py)]^{2+}$, $[Mn^{IV}(O)(N4py)]^{2+}$, and $[Mn^{IV}(O)(2pyN2Q)]^{2+}$ are from reference [1].

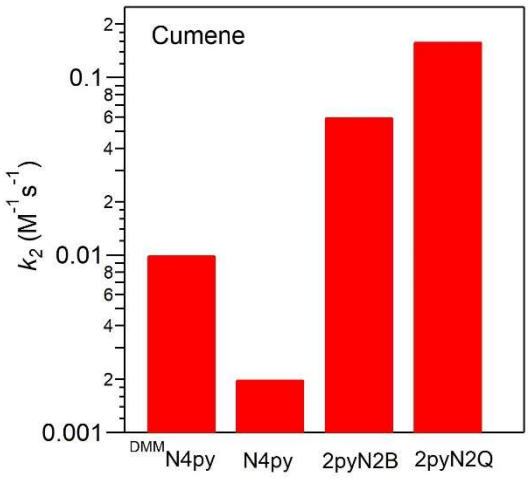

Figure S19. Comparison of second-order rate constants for cumene oxidation by $[Fe^{IV}(O)(^{DMM}N4py)]^{2+}$, $[Fe^{IV}(O)(N4py)]^{2+}$, and $[Fe^{IV}(O)(2pyN2B)]^{2+}$. Data taken from references [3], [4], and [5], respectively.

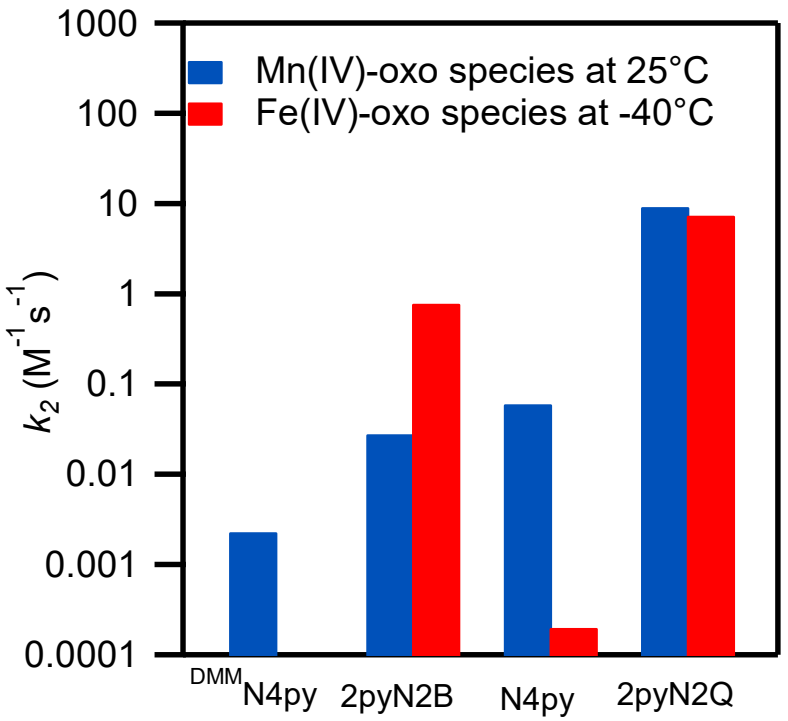

Figure S20. Comparison of the rates of reaction of thioanisole with oxomanganese(IV) at 25ºC and oxoiron(IV) species at -40ºC supported by N4py and its derivatives. Oxoiron(IV) species (excluding ^{DMM}N4py) are shown in red, oxomanganese(IV) species are shown in blue.

S.3 ***Analysis of Multiline EPR Signal in the EPR Spectrum of [Mn^{IV}(O)(2pyN2B)]$^{2+}$.*** The perpendicular-mode EPR spectrum of [Mn^{IV}(O)(2pyN2B)]$^{2+}$ shown in Figure 3 shows a 16-line Mn^{III}Mn^{IV} dimer impurity at g = 2.0, which presumably results from the thermal decay of [Mn^{IV}(O)(2pyN2B)]$^{2+}$. Because both the Mn^{III}Mn^{IV} dimer and Mn^{IV}-oxo species show EPR signals in the g = 2.0 region, spin quantification cannot be used to determine the exact amount of Mn^{III}Mn^{IV} dimer present in the sample. However, using a previously published protocol, we were able to prepare a separate EPR sample for the closely-related [Mn^{III}Mn^{IV}(μ-O)(^{DMM}N4py)$_2$)]$^{2+}$ complex.[6] Recording conditions were 9.637 GHz microwave frequency, 2.0 mW microwave power, 4.55 G modulation amplitude, 100 kHz modulation frequency, and 141 ms time constant. As seen in Figure S21, the Mn^{III}Mn^{IV} signal in the [Mn^{IV}(O)(2pyN2B)]$^{2+}$ sample (Figure 3 and

S21) is very weak, consistent with our assumption that this signal represents a small fraction of Mn in the sample. Spin quantification was used to estimate that 4% of the total amount of Mn in solution is present as a dimer. However, it must be emphasized that this value is likely over estimated due to the overlapping Mn^{IV}-oxo signal at $g = 2.0$.

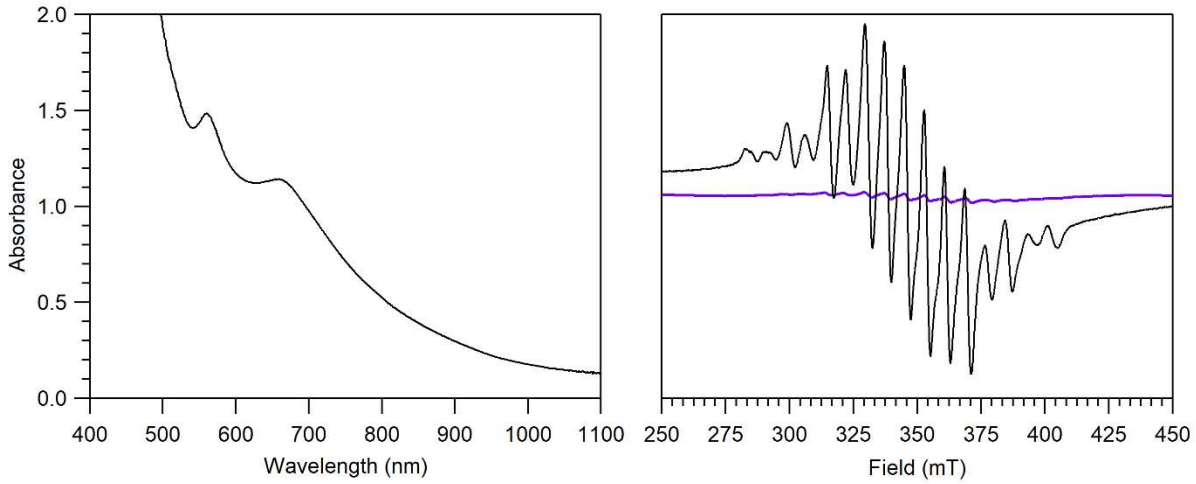

Figure S21. A sample of $[Mn^{III}Mn^{IV}(\mu\text{-}O)(^{DMM}N4py)_2)]^{2+}$ was prepared in TFE, according to a previously published protocol.[6] Left: Electronic absorption spectrum of 10mM $[Mn^{III}Mn^{IV}(\mu\text{-}O)(^{DMM}N4py)_2)]^{2+}$. Right: 5mM $[Mn^{III}Mn^{IV}(\mu\text{-}O)(^{DMM}N4py)_2)]^{2+}$ in TFE (black trace) and 10mM $[Mn^{IV}(O)(2pyN2B)]^{2+}$ (purple trace, see Figure 3 for full spectrum). The $Mn^{III}Mn^{IV}$ signal in the purple trace is very weak compared to that of pure dimer of a closely related complex, suggesting it represents a small fraction of the Mn in the sample.

Table S4. Cartesian Coordinates for $[Mn^{IV}(O)(2pyN2B)]^{2+}$ Optimized by DFT Computations.

Atom	x	y	z
Mn	-0.00097035663382	0.23022457549271	-0.60243137675133
O	-0.04306675263990	0.41759964354642	1.05757272577181
N	0.12312599294241	0.05209860938857	-2.76588936855174
N	-1.92537700337637	0.38798726502742	-1.01215777214240
N	-3.59790345194925	0.54791581668974	-2.48756868676180
N	2.03351311259927	0.19207611460063	-0.82871069685590
C	-1.18204945278439	0.49972488920407	-3.36974985003010
C	-2.25326594340202	0.45110494286929	-2.31182392906430
C	-3.11611281567467	0.44883307937452	-0.28213349948636
C	-4.18188741045777	0.55207571394838	-1.20819736504342
C	-4.34532616980656	0.66368366218846	-3.74916862061893
C	-5.52114228223479	0.63817473534084	-0.80160693064979
C	-5.75051966823919	0.61920009892809	0.57801880681712
C	-4.68930541040975	0.51757296202600	1.50995945560605
C	-3.35574180494736	0.42905981131732	1.10180566281541
C	1.26224086630206	1.04110661510544	-2.94253424264619
C	2.42377329272527	0.54804749782097	-2.08178453176260
C	2.94676363710445	-0.16030953482708	0.09703033951315
C	4.31300866010966	-0.18077501026841	-0.20889191601382
C	4.72738146774743	0.16919548069245	-1.50035872994253
C	3.76807115771406	0.54480543629904	-2.45715933324680
N	-0.04149917842910	-1.73979026076264	-0.72744191586075
N	0.06152483467532	-3.61716060490518	-1.93770638688253
N	0.24751165318749	2.20158826105203	-1.09766955836672
C	0.48067963461705	-1.36856479608596	-3.11702148028336
C	0.14069421318853	-2.26010919290603	-1.95108481057025
C	-0.25239950581609	-2.80834997724692	0.14866719046906
C	-0.18781184761323	-4.00275311477163	-0.60852905838872
C	0.22222391257045	-4.55030329730928	-3.06341006566399
C	-0.35817784256391	-5.26755054284148	-0.02766353356259
C	-0.59536206581882	-5.28751806719751	1.35053933401939
C	-0.65894739491675	-4.09674907911723	2.11459469193215
C	-0.49075605074528	-2.83747260251772	1.53266296304841
C	0.80846342768646	2.36282152934957	-2.32575341691500
C	-0.10697893531683	3.27305064587622	-0.36241289596025
C	0.07972223732698	4.57363031454978	-0.84688521774973
C	0.64124289912801	4.75366862200693	-2.11707209644554
C	1.01711954311395	3.62947783750489	-2.87338531447491
H	-1.06313684833705	1.53627388209681	-3.73266220812823
H	-1.43491929249199	-0.12152843671609	-4.24601340631399
H	-3.65473636236250	0.58065964176494	-4.59891029969759
H	-5.09222933737218	-0.14379713371336	-3.80654054569848
H	-4.85541401842777	1.63941700452368	-3.78839164835261
H	-6.34625517979383	0.71979122642154	-1.51439155894029
H	-6.77835380052529	0.68769613439485	0.94648681642882
H	-4.92340810320859	0.51035019138015	2.57884916388937
H	-2.52760000933402	0.35600220883053	1.81094144615493
H	1.56337475126307	1.16732751712954	-3.99676516403551
H	2.54872785600703	-0.41122815625696	1.08383973531408
H	5.03595047461784	-0.46203133201947	0.56168558301908
H	5.78966448708975	0.15885500202338	-1.76426687211040
H	4.06508999271172	0.83601807437826	-3.46893509842401
H	1.56592498088444	-1.41613115355139	-3.31970772680898
H	-0.03464381955914	-1.67896603837193	-4.04172444769668

H	0.36828855310304	-3.98772953495021	-3.99500167409681
H	-0.68108868284121	-5.17440771200321	-3.15205811694312
H	1.09799621691548	-5.19500574745335	-2.88691866134319
H	-0.30813373796553	-6.19131073740234	-0.61017035980153
H	-0.73431568679252	-6.25004281037415	1.85167455662552
H	-0.84489297726867	-4.16843447372878	3.19041446127178
H	-0.53263111095093	-1.91215593833031	2.11214631976379
H	-0.53033678368097	3.05376430540777	0.62126924255412
H	-0.20856956527432	5.42780415723255	-0.22845301083924
H	0.79469877901072	5.76019492672753	-2.51846081108764
H	1.46837432489423	3.74143870300788	-3.86344842155496

Table S5. Cartesian Coordinates for $[Mn^{IV}(O)(N4py)]^{2+}$ Optimized by DFT Computations.

Atom	x	y	z
Mn	-0.23633646371276	0.60328106557608	0.91458632057475
O	0.18624376401618	2.16543911466274	1.34036633424372
N	0.43421312984041	-0.30223186612636	2.58178711605595
N	1.48550802625649	0.12612225028571	-0.00871225846301
N	-2.13345191346404	0.58217995021707	1.62364209011379
N	-1.13231987443518	0.99140771618478	-0.86013086676241
C	0.19280989312914	-1.63978889468179	2.67260674519352
C	-2.89068861939440	-0.37358888148184	1.01662994780429
C	1.52323143716089	-1.10017122781278	-0.60083281027177
N	-0.75561114458402	-1.37907045842057	0.37864818316473
C	-1.98966456115381	-0.00354333078124	-1.22243977058740
C	-0.95053402681276	2.06503946821093	-1.65612294114020
C	-2.65801692876309	1.36371822614909	2.58919448782632
C	0.70673286844912	-2.38987967925658	3.73505125332755
C	-4.77084020085366	0.21067269832217	2.39962228836442
C	2.70504279608784	-1.58517051831976	-1.16928802459247
C	-0.72565828032329	-2.22893761985374	1.61780964579224
C	0.20330093301152	-1.84556081888592	-0.68091191821195
C	2.59228030870613	0.90694435631226	0.02227862549224
C	1.16547160317044	0.32802118519923	3.53278476714803
C	1.69192573777111	-0.36486872913064	4.62361351452081
C	-2.15112277463869	-1.05966643243667	-0.13091770227945
C	3.85584864159685	-0.78350180834461	-1.13998173798026
C	-2.49237797213144	1.15057344709359	-3.27384216584020
C	1.46542307679809	-1.74501077507588	4.72287947631398
C	-1.62177108050751	2.17501320672440	-2.87941922646567
C	3.79625656122614	0.48327276814988	-0.54207701022019
C	-3.98528165746621	1.20159842977850	3.00236407164961
C	-4.21855129621158	-0.59074952149901	1.38409998710551
C	-2.68653290246197	0.04151834506394	-2.43002445645423
H	-0.26616466582444	2.82884032132236	-1.27738044224007
H	-1.98877902552188	2.12114343107462	3.00609110945982
H	0.50913448405773	-3.46466241608803	3.79268959287058
H	-5.80944545366317	0.06179030104581	2.71054836781407
H	2.72333300081392	-2.57475770871569	-1.63509472725440
H	-0.43766175703439	-3.26560942655779	1.37412950135833
H	-1.74887797460305	-2.26812757268335	2.03077332365422
H	0.35708302000294	-2.93595996226629	-0.61621153454300
H	-0.25138344137920	-1.64223567219133	-1.66671509006290
H	2.46571768647782	1.87365397331598	0.51728910732544
H	1.30628691188510	1.40154036252504	3.37638398497758

H	2.27461644915710	0.17247661406573	5.37716816283863
H	-2.69434606145817	-1.94713761182281	-0.49690950629178
H	4.78935767645011	-1.14625842975516	-1.58108344123076
H	-3.02399888189002	1.21174032225063	-4.22829780332844
H	1.87444550117795	-2.31657008641444	5.56196721762989
H	-1.46246302110947	3.05695617483135	-3.50617150268894
H	4.67188967138323	1.13733218222497	-0.50499241062410
H	-4.39142678698938	1.84992598098266	3.78387072268048
H	-4.81371305336651	-1.36461459557718	0.89026864591723
H	-3.36905835887215	-0.76687184739008	-2.70940224368414

References

1. Massie, A. A.; Denler, M. C.; Cardoso, L. T.; Walker, A. N.; Hossain, M. K.; Day, V. W.; Nordlander, E.; Jackson, T. A., Equatorial Ligand Perturbations Influence the Reactivity of Manganese(IV)-Oxo Complexes. *Angew. Chem., Int. Ed. Engl.* **2017,** *56* (15), 4178-4182.
2. Leto, D. F.; Ingram, R.; Day, V. W.; Jackson, T. A., Spectroscopic properties and reactivity of a mononuclear oxomanganese(iv) complex. *Chem. Commun.* **2013,** *49* (47), 5378-5380.
3. Rana, S.; Dey, A.; Maiti, D., Mechanistic elucidation of C-H oxidation by electron rich non-heme iron(iv)-oxo at room temperature. *Chem. Commun.* **2015,** *51* (77), 14469-14472.
4. Kaizer, J.; Klinker, E. J.; Oh, N. Y.; Rohde, J.-U.; Song, W. J.; Stubna, A.; Kim, J.; Münck, E.; Nam, W.; Que Jr., L., Nonheme FeIVO Complexes That Can Oxidize the C−H Bonds of Cyclohexane at Room Temperature. *J. Am. Chem. Soc* **2004,** *126* (2), 472-473.
5. Mitra, M.; Nimir, H.; Demeshko, S.; Bhat, S. S.; Malinkin, S. O.; Haukka, M.; Lloret-Fillol, J.; Lisensky, G. C.; Meyer, F.; Shteinman, A. A.; Browne, W. R.; Hrovat, D. A.; Richmond, M. G.; Costas, M.; Nordlander, E., Nonheme Fe(IV) Oxo Complexes of Two New Pentadentate Ligands and Their Hydrogen-Atom and Oxygen-Atom Transfer Reactions. *Inorg. Chem.* **2015,** *54* (15), 7152-7164.
6. Lee, Y.; Jackson, T. A., Ligand Influence on Structural Properties and Reactivity of Bis(μ-oxo)dimanganese(III,IV) Species and Comparison of Reactivity with Terminal MnIV-oxo Complexes. *ChemistrySelect* **2018,** *3* (47), 13507-13516.